Photochromism and Photomagnetism in 1,4-bis(4,5-diphenyl-imidazolyl)benzene Chromophores: Water Assisted π-stacks for the Generation of Stable Free Radicals in Solid State

Subhajit Saha,[a] Sudipta Khamrui,[b] Rajib Moi,[a] Anakuthil Anoop,[a] Vladimir Chernyshev,[c] Debamalya Banerjee[b] and Kumar Biradha*[a]

[a] S. Saha, R. Moi, Dr. A. Anoop and Prof. K. Biradha
Department of Chemistry
Indian Institute of Technology (IIT), Kharagpur
Kharagpur, West Bengal-721302, India
E-mail: kbiradha@chem.iitkgp.ac.in
[b] S. Khamrui and Dr. D. Banerjee
Department of Physics
Indian Institute of Technology (IIT), Kharagpur
Kharagpur, West Bengal-721302, India
[c] Dr. V. Chernyshev
Department of Chemistry
Moscow State University
Moscow-119992, Russia

Abstract: Photochromism and photomagnetism are two important features for the generation of smart materials that are of utility for optical switches and memory devices. Very few materials that exhibit both the features at room temperature are known to date, the reported ones mostly contain metal-ions to assist the electron transfer with photo stimuli. Herein, we report a new class of organic materials that show photochromism and photomagnetism at room temperature due to the generation of free radicals in the solid-state. 1,4-bis(4,5-diphenyl-1H-imidazol-2-yl)benzene (**BDPI**) was found to acts as organic photomagnet without use of any traditional photochromic couplers or radical containing moieties. Solvent molecules (eg. water and DMSO) form hydrogen bonds with the imidazole rings which act as binding glue in stacking of 1,4-bis(imidazolyl)benzene moieties *via* π···π interactions. These interactions found to play a significant role in promoting strong spin-spin interaction in the solid-state which can be inferred from the appearance of broad EPR signal, whereas a sharp signal appeared only after irradiation. The sharp signal indicates formation of paramagnetic free radicals which influence antiferromagnetic exchange interactions with weakening of the magnetic susceptibility significantly. This work provides a new direction in the ongoing research of photochromic and photomagnetic materials, where a simple 1,4- bis(imidazolyl)benzene system changes its color, radical activity and magnetic behavior with photoirradiation.

Introduction

Stable organic radicals owe an increasing demand as a promising building blocks of functional materials due to their unique electronic and physical properties.[1-3] Over the years, many organic radicals have been synthesized to explore solid-state magnetism, where weak noncovalent interactions significantly influence the interactions between unpaired spins.[4-7] Among the numerous radical families, nitrogen-rich benzotriazinyl and benzimidazole radicals and sulfur rich thiazyl radicals have received more attention given their excellent magnetic activity and stability at room temperature.[8-11] Photo-magnets are special class of magnetic materials for which light acts as an external stimulus for switchable magnetic behavior.[12-15] This phenomenon was observed for many years in metals (Cu, Al) and metal oxides (ferrites, garnets), after that Prussian Blue analogs (PABs) was introduced by Hashimoto and coworkers as an efficient photomagnet in late 90s.[16-18] More recently, a new class of inorganic-organic hybrid material had been developed by incorporating photochromic moiety into 3d-4f heterobimetallic complexes that show photomagnetism at room temperature.[19,20] The photomagnetism was shown to originate due to photoinduced electron transfer (PET) from electron-rich (18-crown-6) or electron-deficient (viologen derivatives) organic moieties to redox active metal ions. Diarylethene and azobenzene based photochromic couplers are the common units in most of the organic photomagnets, where photoisomerization switches magnetic interactions between the radicals.[21,22] To date, no organic material which exhibit photochromism and photomagnetism together without altering its structural identity is reported to the best of our knowledge. Such materials are very essential for fundamental understanding as well as for practical applications in optical switches and memory devices.

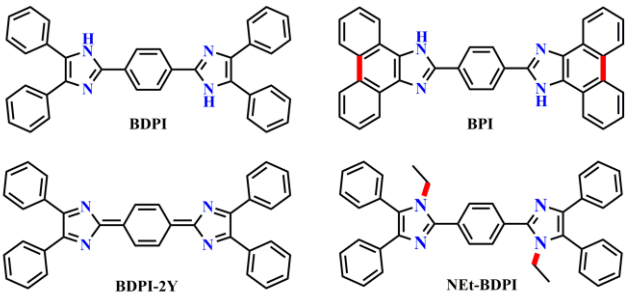

Scheme 1. Chemical structure of the 1,4-bis(imidazolyl)benzene system and their derivatives.

1,4-bis(imidazolyl)benzene derivatives are well known chromophores for their excellent photophysical and photochemical properties in solution state.[23,24] Kaftory and Speiser have shown that the acetonitrile, water and acetic acid solvates of 1,4-bis(imidazolyl)thiophene exhibit solid-state photochromic, piezochromic and thermochromic properties.[25] Further, we have shown earlier that the influence of *cation···π, COO···H-N⁺ and COO···N⁺ interactions* in the generation of photochromic organic semiconductor through light induced radical formation in the solid state.[26] The photochromic nature of the 4,4'-bipyridinium cations (also termed as viologens) and many other interesting crystalline materials have been studied to explore their potential applications as smart photoswitchable devices.[27-29] Very recently, Guo and coworkers have reported that 4,4'-bipyridinium cation exhibits reversible photochromism with semiconductivity, where the coloration and decoloration process was triggered by light.[30] They have concluded that strong *cation-π* interactions assisted in quick electron transfer in these transformations resulting in the variation of colors and corresponding semiconductivity values. The organic materials containing bis(imidazolyl)benzene moieties are anticipated to exhibit such photochromism through the radical generation.

In accordance, to study photochromism through radical generation further 1,4-bis(imidazolyl)benzene was selected which is an interesting chromophore as the oxidized form of which was well studied for photochromism in solution state due to the light induced generation of free radicals.[31-33] In the oxidized form, a reversible transformation of singlet quinoid state to triplet biradical state was observed by EPR studies. However, the nature of its non-oxidized form and its behaviour in the solid state was not addressed to date. In this context, 1,4-bis(4,5-diphenyl-1H-imidazol-2-yl)benzene (**BDPI**) and its planar counterpart 1,4-bis(1H-phenanthro[9,10-d]imidazol-2-yl)benzene (**BPI**) were chosen for the detailed study on their photochromic, radical and EPR activities in the solid state (Scheme 1). For each system, two different solvates with water and DMSO/DMF were prepared to understand the solvent dependency on chromogenic behavior. Interestingly, **BDPI** found to show photochromism, whereas **BPI** remains photo-silent. Further, two modified analogues of BDPI, oxidized form (**BDPI-2Y**) and N-alkylated form (**NEt-BDPI**), were also analysed in detail to understand the importance of -NH group on the imidazole ring behind photochromism. The materials were thoroughly analysed using solid-state electron paramagnetic resonance (EPR) and superconducting quantum interference device (SQUID) to understand their radical generation, photochromic and photo-magnetic behaviours, and correlated these properties with their structural features. Further, spin density distribution calculations were used to understand the difference in radical activity between the two types of stacks of BDPI units.

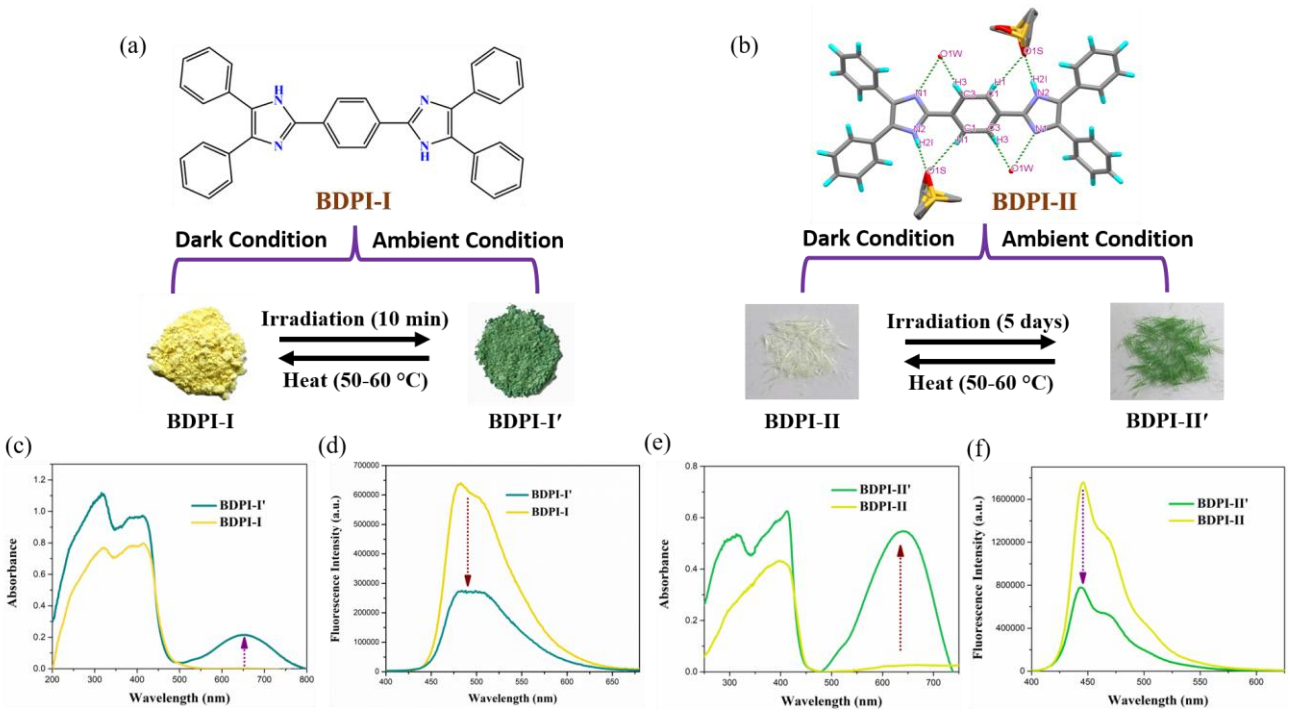

Figure 1. Photochromism in (a) **BDPI-I** and (b) **BDPI-II**; (c) UV/Vis diffuse reflectance and (d) solid-state fluorescence spectra of **BDPI-I**; (e) UV/Vis diffuse reflectance and (f) solid-state fluorescence spectra of **BDPI-II**.

Results and Discussion

BDPI and **BPI** were synthesized according to the Devidson method.[34] Benzil or 9,10-phenanthroquinone, terephthaldehyde and ammonium acetate were dissolved in hot glacial acetic acid and refluxed for 5-6 hours. Solid products of BDPI and BPI were obtained after washing with excess amount of water and dried in air. The assynthesized BDPI (**BDPI-I**) and BPI (**BPI-I**) were further characterized through ^{1}H-NMR, FT-IR and HRMS analyses (Figure S1-S5). Crystallization of **BDPI-I** from DMSO/water (4:1) solvent system yields large needle shaped crystals **BDPI-II** (BDPI.2DMSO.H_2O). The crystallization of **BPI-I** from DMF/water (4:1) solvent system resulted in plate shaped crystals of **BPI-II** (BPI.2DMF). The crystals structures of **BDPI-II** and **BPI-II** were determined and thoroughly analysed in terms intermolecular interactions in their crystal lattices. Pertinent crystallographic details along with hydrogen bonding parameters are given in Table S1 and S2 (Figure S6).

It is interesting to note here that the solid product of **BDPI** initially appeared in yellow color but it turned into deep green during filtration and drying under ambient condition. This change in color with in few minutes indicated the photochromic nature of **BDPI-I**. To evaluate the effect of light in the color change, the synthesis and workup procedures were carried out under dark condition. This process resulted in bright yellow colored product (Figure 1a) which turned to green color solid (**BDPI-I'**) upon exposure to sunlight or low-power white-light source light emitting diode (LED) within few minutes. Instead of applying white light, we have used different UV lights (UV-A and UV-B) and lights of a particular range of wavelength (red, green and blue), but in all cases the color change was occurred (Figure S7). This clearly indicates that the as-synthesized BDPI (**BDPI-I**) exhibits photochromism irrespective of any light source. Further, the green-colored material **BDPI-I'** was found to be stable and remains green for more than a month in room light or in dark condition but transformed into yellow upon heating at 50-60 °C for 4-5 minutes (Figure S8). Such reversible transformation of colour changes was found to occur in similar manner for four consecutive cycles which becomes somewhat sluggish after four cycles. The powder X-ray diffraction patterns, IR and Raman spectra of both the forms found to be identical (Figure S9), however they found to exhibit different solid-state diffuse reflectance spectra (DRS) and luminescence properties.

In DRS, **BDPI-I** shows two absorption bands at 310 nm and 400 nm, whereas the **BDPI-I'** exhibits one additional absorption band at 650 nm (Figure 1c). The optical band gap for both the materials were determined from Tauc's plot using the equation for the direct and indirect band gap.[35,36] **BDPI-I'** shows a relatively lower value of 1.64 eV and 1.56 eV for direct and indirect band gap, whereas the **BDPI-I** shows quite higher value of 2.72 eV and 2.53 eV, respectively (Figure S10a,b). Origin of the absorption band at 310 nm is typically from the side phenyl rings of **BDPI** whereas the longer wavelength band at 400 nm can be attributed to the absorption of whole bis(imidazolyl)benzene moiety.[23] The solid-state luminescence spectra **BDPI-I'**, upon excitation at 310 nm and 400 nm, shows a common emission maximum at 500 nm with half of an intensity compared to the nonirradiated yellow material (Figure 1d). Additionally, the solid-state fluorescence lifetime was calculated for **BDPI-I** and **BDPI-I'**, where the **BDPI-I'** exhibits a shorter lifetime by 1.6 ns (Figure S10c). Therefore, the quenching in emission intensity with shorter lifetime for the **BDPI-I'** replicate strong non-radiative decay pathway in organic radicals, caused by self-absorption of photoinduced radical or electron exchange between the photogenerated radical and the fluorophore.[37,38]

Similar type of characteristics was observed for DMSO-H_2O included crystalline **BDPI-II**; the white-colored crystals grown under dark condition converted into deep green crystals (**BDPI-II'**), albeit with prolonged irradiation for five days (Figure 1b and Figure S11a). The two forms **BDPI-II & BDPI-II'** show similar FTIR and PXRD pattern (Figure S11b,c), whereas **BDPI-II'** exhibited distinguishable absorbance spectra with a generation of a broad band at 650 nm (Figure 1e) which is absent in **BDPI-II**. In solid state emission spectra, hypsochromic shift of 45 nm was observed for **BDPI-II** with respect to **BDPI-I**, that could be the effect of presence of different solvent molecules which influences the stacking of chromophores in the crystal lattice (Figure S11d).[39,40] A similar fluorescence quenching was observed in case of **BDPI-II'** in comparison with **BDPI-II**, which suggests the analogous effect of light on both **BDPI-I** and **BDPI-II** forms (Figure 1f).

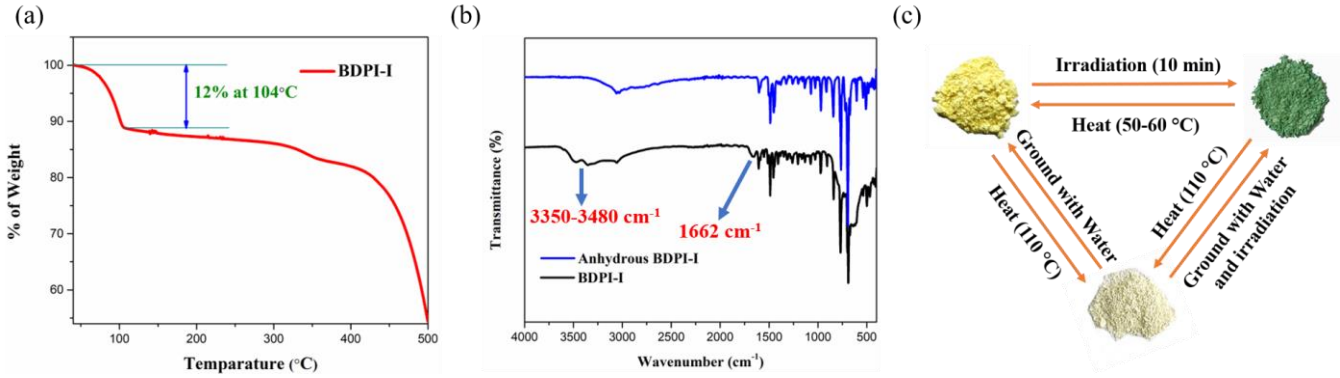

Figure 2. (a) TGA-curve of **BDPI-I**; (b) FT-IR spectra of irradiated and anhydrous form of **BDPI-I**; (c). tuneable photochromism in **BDPI-I.**

In order to explore the reversibility of photochromism under heat, the TGA of both the forms were evaluated. The TGA plot of **BDPI-I** shows the weight loss of ~12% at 104°C (Figure 2a). This loss indicates the possible presence of four water molecules per BDPI unit which might have been included in the **BDPI-I**. The FTIR exhibits broad signals at 3350-3480 cm^{-1} and 1662 cm^{-1} due to the -OH stretching and -OH bending respectively (Figure 2b), which is in support of presence of H_2O molecules. The TGA of **BDPI-II** shows weight loss of 2% and 21%, at 107 °C and 161 °C respectively, which correspond to the loss of H_2O and DMSO respectively (Figure S12). The TGA shows that both the materials are stable up to 100 °C and therefore their irradiated forms (**BDPI-I'** and **BDPI-II'**) of both are heated up to 50-60 °C, which resulted in the generation of the original forms in yellow color.

It was further found that the anhydrate of **BDPI-I** can be prepared by heating it at 110 °C for 30 mins. The FT-IR spectra of the heated material shows that signals related to water molecules were vanished which confirms the formation of anhydrous **BDPI-I**. The PXRD patterns of anhydrate **BDPI-I** found to be different from that of its parent material (Figure S13). The anhydrous **BDPI-I** exhibits off-white color, but doesn't show any color change upon irradiation. However, grinding of the anhydrate with a drop of water changes its color to yellow which changes into green immediately with irradiation (Figure 2c). Thus, it can be inferred that the presence of water playing a significant role in photochromic property of **BDPI-I**. Despite of several trails we could not obtain single crystals of **BDPI-I**. However, Rietveld analyses of its powder X-ray Diffraction pattern using Pawley fitting method resulted in a possible model structure for **BDPI-I**. The PXRD of **BDPI-I** was indexed in two syngonies: orthorhombic or monoclinic (TableS3). We considered one model structure that provided the most reasonable arrangement of molecules in the monoclinic unit cell $P2_1/n$ with χ^2 = 27.8 and $R_p/R_{wp}/R_{exp}$ = 0.055/0.075/0.015 (Table S4 and Figure S14). The asymmetric unit is composed of one BDPI molecule and four water molecules. On the other hand, **BDPI-II** crystallizes in $P2_1/c$ space group and the asymmetric unit is composed of half unit of BDPI, one disordered DMSO with two orientations and one water molecule of half occupancy. In both the forms, the imidazole ring of BDPI was involved in hydrogen bonding (N−H···O and O−H···N) with the solvent molecules as shown in figure S6a and S15a. Further, BDPI molecules form stacks, however considerable differences were observed in the interactions between the stacks and arrangement of stacks with respect to neighbors (Figure 3b,d). In **BDPI-I**, two adjacent 1,4-bis(imidazolyl)benzene moieties are stacked in off-set along the length of the molecule, *via* π-π interaction between the imidazole ring and central phenylene ring with the centroid-to-centroid distance of 3.51 Å (Figure 3a). The terminal phenyl rings interact with the imidazole rings *via* similar π-π interaction with a centroid-to-centroid distance of 3.664 Å. In contrast, the stacks in **BDPI-II** contains edge-to-face π-π interaction with the distance (carbon of edge to centroid) of 3.442 Å between the terminal phenyl ring and the imidazole ring (Figure 3c). The central phenylene rings have weak π-π interactions as the only one of their C-H groups overlap on each other as the stacks formed in totally slipped mode along the width of the molecule.

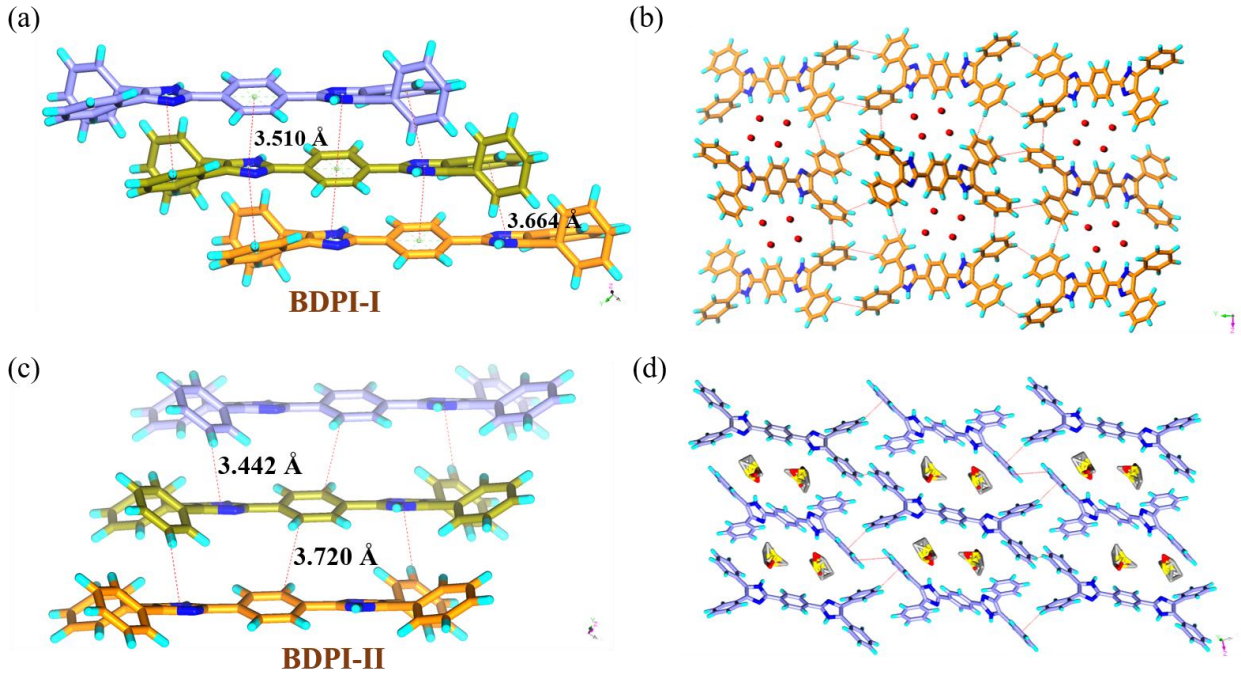

Figure 3. (a) Molecular stacking observed in **BDPI-I** and (c) **BDPI-II**; solvent included two-dimensional arrangement *via* weak non-covalent interactions in (b) **BDPI-I** and (d) **BDPI-II**.

The solid state EPR studies have been conducted to understand the differences between the photophysical properties of **BDPI-I** *vs* **BDPI-I'** and **BDPI-II** *vs* **BDPS-II'** which exhibited quenching of fluorescence and shortening of the fluorescence lifetime upon irradiation. Yellow-colored **BDPI-I** shows a broad band at higher g value around 2.22 with peak-to-peak width of ≈100 mT (Figure 4a). Such high g value with broad EPR-signal is the signature of strong radical activity, mostly observed in metal-oxides where redox-active metal centres placed in close proximity.[41-43] BDPI as a non-metallic system confirmed through XPS analysis (Figure S16), the broad signal is being appeared through the spin-spin interaction of the π-radical centres, those are in close proximity. Interestingly, **BDPI-I'** exhibit a totally different radical activity compared to its parent material. Along with the broad EPR signal, a very sharp signal appeared at g=2.001 with ΔH_{pp} value of 1 mT, which was absent for the parent material. The sharpness of the signal and g-value (2.003 for free electron) indicates the photo-generated free radicals stabilized through the π-aromatic moieties in **BDPI-I'** and, hence, promotes the photochromism. The reversible color change was further verified through EPR activity, heating at 50-60 °C of **BDPI-**I' transformed into pale yellow colored **BDPI-I''** where very weak radical signal was observed for both the broad and sharp signals (Figure S17a).

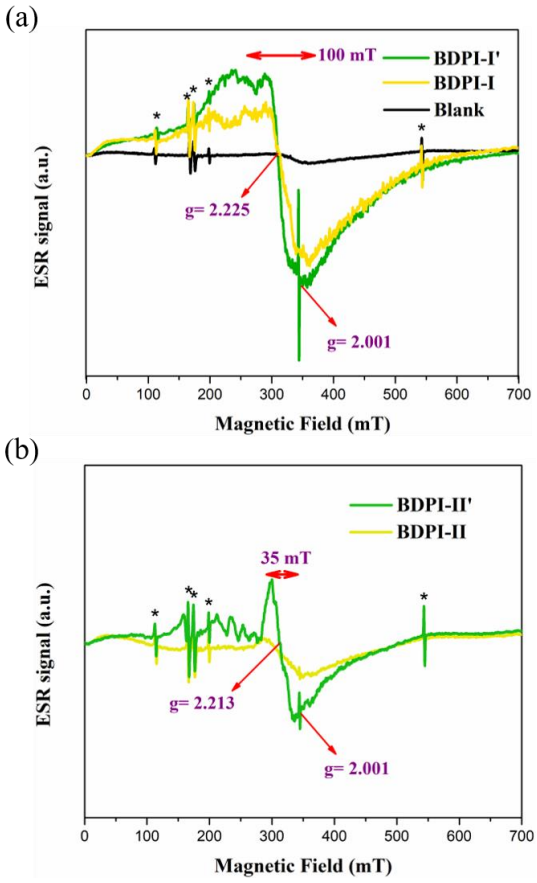

Figure 4. (a) Solid-state EPR-spectra of non-irradiated and irradiated form of **BDPI-I** and (b) **BDPI-II**. For the EPR signals coming from blank EPR tube are indicated by *.

No such signals correspond to radical generation is observed in the EPR spectra of toluene or benzene solution of BDPI (Figure S17b). This fact highlights the importance of cooperative interactions which exists in the **BDPI-I**. It is interesting to note here that the anhydrate form of **BDPI-I** does not exhibit any such significant radical activity, highlighting the presence of water in **BDPI-I** (Figure S17c). Similarly, **BDPI-II** and **BDPI-II'** also exhibited signals around the g value of 2.21 with peak-to-peak width of ≈35 mT, albeit **BDPI-II'** shows an intensified signal (Figure 4b). The signal corresponding to free radical that is at g=2.001 also appeared in **BDPI-II'**, it is sharp but lower in intensity than that of **BDPI-I'**. The lower ΔH_{pp} value (100 mT *vs* 35 mT) of the broad radical signal and weaker free radical signal for **BDPI-II'** indicate a considerable difference in spin-spin interaction in the forms of **BDPI-I** and **BDPI-II** given the differences in their stacking interactions. As a result, the photochromic response is faster (5 mins) in **BDPI-I** compared to **BDPI-II** (5 days) which doesn't contain strong π-π interactions.

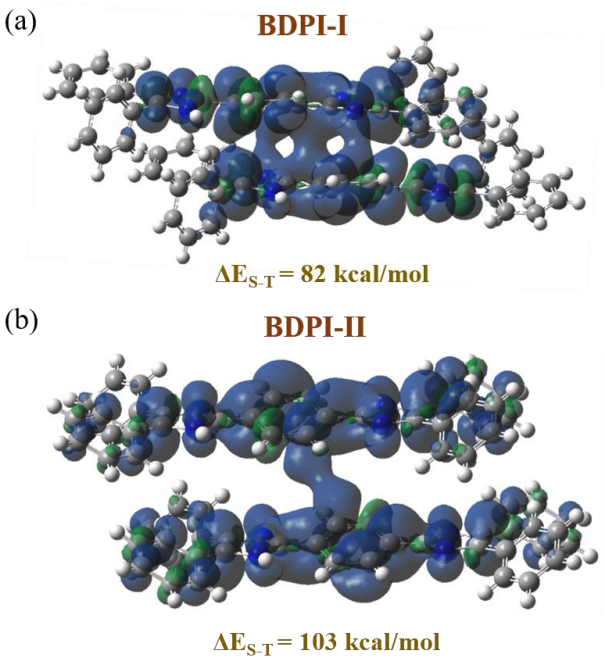

Figure 5. Spin-density distribution plot of (a) **BDPI-I** and (b) **BDPI-II**.

The significant difference in the stacks of **BDPI-I** and **BDPI-II** is face-to-face interaction in **BDPI-I** and edge-to-face interaction in **BDPI-II**. In order to understand the differences in these stacking interactions and radical activity, single point energy calculations were performed by considering the dimeric units of the stacks using wB97XD/Def2TZVP basis set with Gaussian 16 program suite.[44,45] These calculations reveal that both the dimers are stabilized by non-covalent interactions as demonstrated by NCI plots using Multiwfn software and exhibits comparable interaction energy values (Figure S18).[46] The spin density distribution pattern was calculated to get some insights on the effect of π-π stacking in intermolecular spin-spin interactions. The energies of the singlet and triplet states of BDPI-dimers were calculated from single point energy calculation using the same basis set, where singlet state calculations were done in restricted mode and triplet state calculations were done in unrestricted mode. For **BDPI-I**, the singlet-triplet energy gap (ΔE_{S-T}) was found to be 82 kcal/mol,

whereas for **BDPI-II** the gap became higher with the value of 103 kcal/mol. In addition to that **BDPI-I** shows delocalization of spin density between the two BDPI molecules, which is less in **BDPI-II** (Figure 5 a,b). Thus, face-to-face stacking in **BDPI-I** is

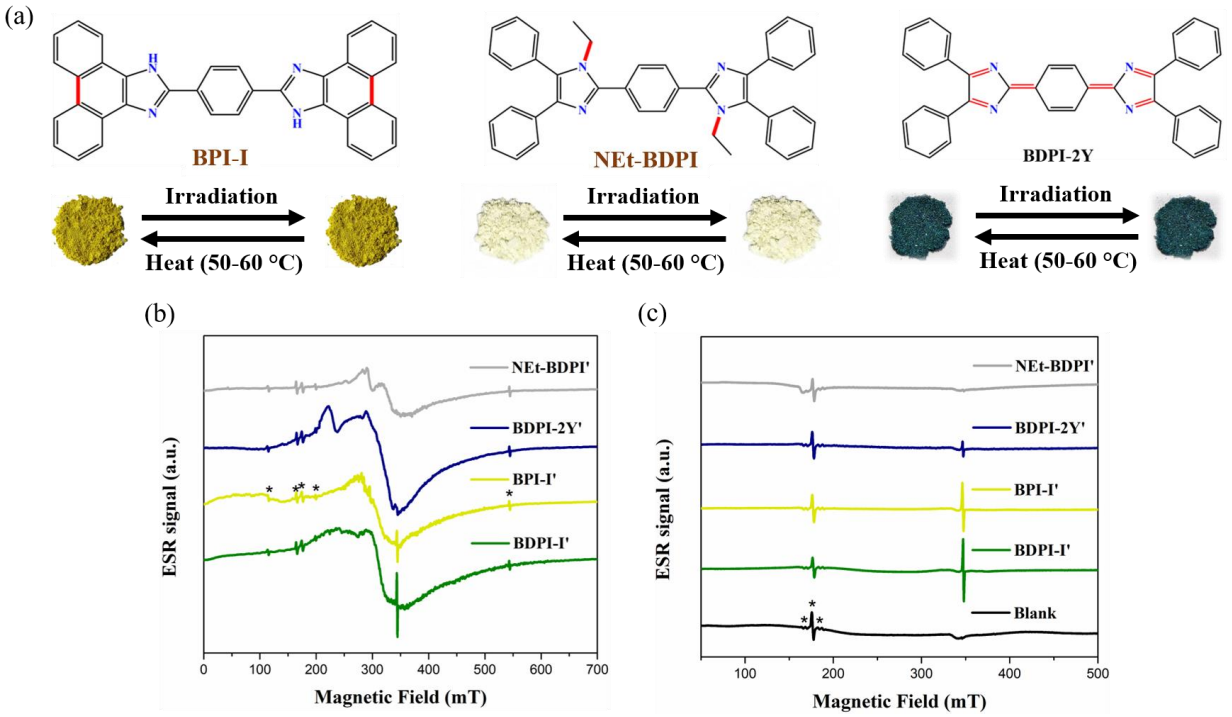

Figure 6. (a) Modified **BDPI**-analogues with control experiments; (b) solid-state EPR spectra of **BDPI**-analogues at 298 K and (c) at 7.6 K.

effective in minimizing the singlet-triplet energy gap, which is also an important criterion for radical stabilization in triplet state. These results are quite significant and in agreement with strong radical activity in **BDPI-I**, which also shows better photochromic response than **BDPI-II**. The existence of the free radical coupled with strong spin-spin interaction prompted us to examine the electrical conductivity of **BDPI-I** before and after irradiation. Therefore, the current-voltage (*I-V*) characteristics of **BDPI-I** and **BDPI-I'** were measured in pallet form using two-probe technique (Figure S19). Surprisingly, we obtained very low conductivity value for the materials in the order of 10^{-10} to 10^{-12} S cm^{-1}, which could be the effect of strong spin-spin interactions in BDPI units similarly observed in phenalynyl radical systems.[47]

Further modifications on 1,4-bis(imidazolyl)benzene moiety have been done to disturb the overall intermolecular interaction followed by spin-spin interaction in solid state. Firstly, **BPI** has been synthesized where the free rotation of the terminal phenyl rings was restricted. Interestingly, no photochromism or thermochromism properties were observed in as-synthesized **BPI-I** (Figure 6a). TGA curve revealed the existence of water molecules in **BPI-I** same as **BDPI-I** (Figure S20a). The irradiated form (**BPI-I'**) and the anhydrate form (heating at 135 °C) didn't show any differences in PXRD pattern or in FTIR spectra, that suggest no significant change in overall packing like **BDPI-I** (Figure S20b,c). Though there was no color change appeared after irradiation, but a considerable quenching of fluorescence intensity and shortening the fluorescence lifetime were observed in **BPI-I'** (Figure S21). These results prompted us to examine the radical activity of the irradiated **BPI-I** in solid-state. Interestingly, both **BDPI-I' & BPI-I'** show almost similar EPR signal, where both the broad and sharp radical signals have existed together with the same g-values (Figure 6b). The possible explanation for no photochromism in the **BPI-I** could be the lack of non-planarity and its effect on molecular packing followed by spin-spin interaction. To find out the molecular packing in **BPI-I**, Rietveld analysis was also performed using the PXRD pattern but due to the poor crystallinity our efforts were not successful. Herein, crystallizing **BPI-I** in DMF-water solvent system produced plate shaped orange colored crystals **BPI-II**, that provided some insights to understand the molecular arrangement as well as supramolecular architecture and its effect on radical activity (Figure S22a). **BPI-II** crystalizes in $P2_1/c$ space group and the asymmetric unit comprises of half unit of BPI, one unit of DMF molecule. DMF molecules are involved in hydrogen bonding interactions with the imidazole ring and placed in between the two BPI units prohibiting the π-stacking of BPI molecules and forms a 2D-herringbone layer (Figure S6b and Figure S22b). **BPI-II** also turned out to be photoinactive same as **BPI-I**. EPR spectra of irradiated form **BPI-II'** didn't show any sharp radical signal corresponding to the free radical and also the broad radical signal became narrower (Figure S22c). Such difference in radical activity could be the lack of π-π interaction in **BPI-II**, which might be present in **BPI-I**. Solid state fluorescence spectra of **BPI-II** also support this agreement, which shows four times lesser intensity than **BPI-I** due to the absence of π-stacking (Figure S22d).

Two more modifications were made on BDPI moiety to examine the effect of imidazole -NH group in originating photochromic property in these systems, one was oxidation of

imidazole ring (**BDPI-2Y**) and the other one was alkylation of imidazole -NH bond (**NEt-BDPI**) (Figure 6a). These syntheses were carried out by reported methods and thoroughly characterized by ^{1}H-NMR, HRMS and FT-IR analyses (Figure S23,24,25,26c). TGA analysis revealed the absence of solvent molecules in the as-synthesized form of **BDPI-2Y & NEt-BDPI** (Figure S26a,b). None of these two exhibited changes of color with irradiation, that clearly indicates the importance of -NH bond in imidazole ring towards photochromism. Moreover, solid-state EPR analysis revealed that the irradiated form **BDPI-2Y'** exhibited the very strong radical signal with ΔH_{pp} value of around 100 mT at g≈2.19, whereas the irradiated **NEt-BDPI'** exhibited an anisotropic broad band (ΔH_{pp}≈63 mT at g≈2.12), but no appearance of sharp radical signal for the free radical at g=2.001 (Figure 6b). We further measured radical activity of all of the irradiated **BDPI** analogues at low temperature i.e. at 7.6 K (Figure 6c). Interestingly, the broad radical signal was completely disappeared in all of them at low temperature, except the free radical signal. For **BDPI-2Y'**, very weak free radical signal observed at low temperature, could be originated from the unreacted **BDPI-I** present in the oxidized form as an impurity. This indicates that the irradiated materials exhibit variable magnetic behavior with respect to temperature. This was analysed further through temperature dependent EPR analysis and measuring the bulk magnetization through SQUID.

In order to investigate the photoinduced magnetism of the photochromic bis(imidazolyl)benzene system, magnetic measurements have been carried out for both the nonirradiated and irradiated forms at a constant field of 0.1 T and the data were corrected for diamagnetism of sample and sample holder. The χT vs T plot of nonirradiated **BDPI-I** revealed the linear increment of magnetic moment with increasing temperature from 10K to 300K, that can be attributed to the antiferromagnetic interactions between the BDPI units (Figure 7b).[8,10] This could be the effect of strong spin-spin interaction takes place between the π-radical centres within the distance of 4 Å to exhibit strong antiferromagnetism. **BDPI-I'** was also having a comparable linear nature in χT *vs* T plot but the difference was its lower magnetic moment value (1.60 emu K/mol) than the non-irradiated one (1.91 emu K/mol) at 300K. χ *vs* T plot also provides similar results, where the irradiated form having lower magnetic moment value all over the temperature range and broadness appeared at around 75K and 160K justified the strong antiferromagnetic ordering of the spin centres after irradiation (Figure 7a).[19,48] These observations clearly suggest the photomagnetic property of **BDPI-I** at room temperature, which is a rare phenomenon in neutral organic chromophores.
In order to get more insights in spin-spin interactions in **BDPI-I'**, the temperature dependent EPR analysis has been performed from 15K to 300K. With temperature increment, the peak-to-peak signal intensity for the free radical getting decreased,

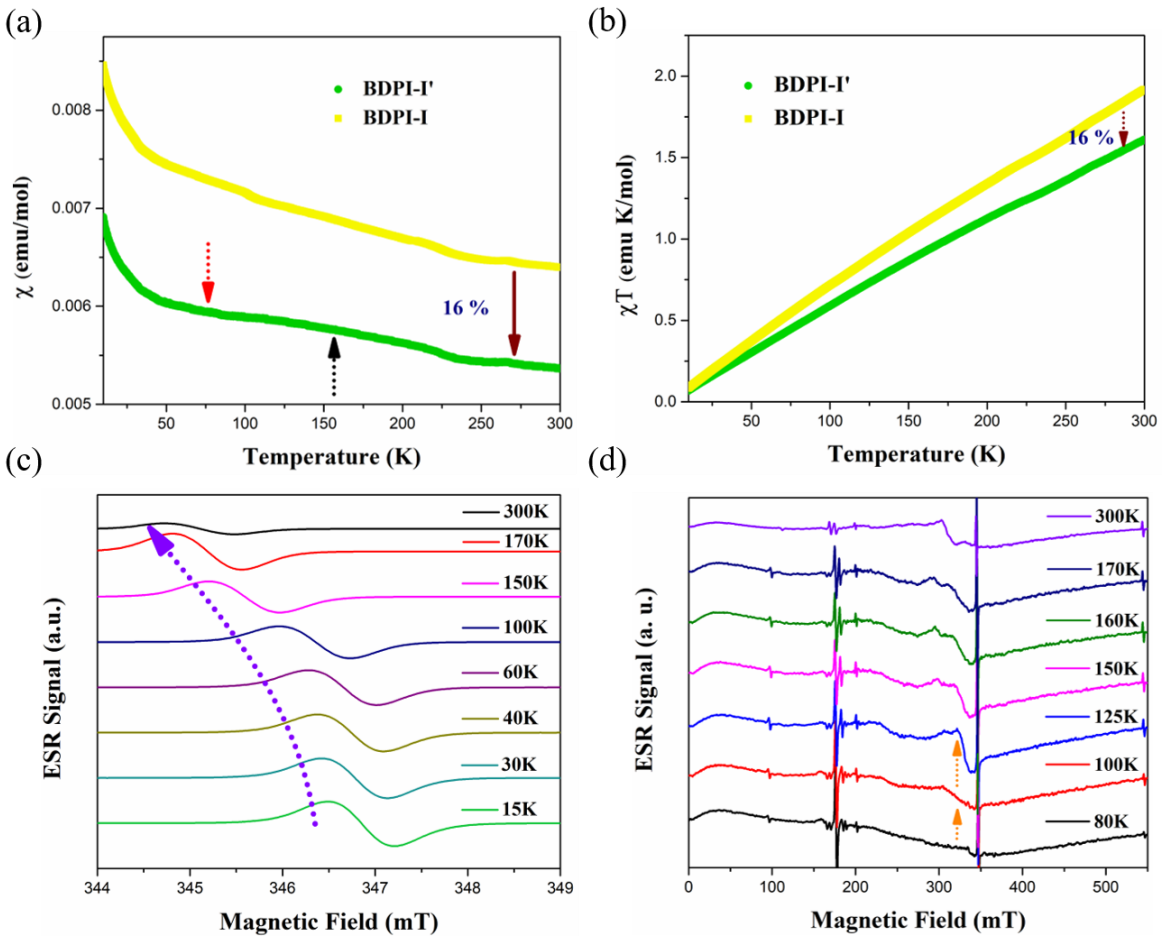

Figure 7. Photomagnetic behavior of **BDPI-I**: (a) χ *vs* T plot and (b) χT *vs* T plot under a magnetic field of 1000 Oe; (c) temperature dependent EPR activity of **BDPI-I'** for the sharp free radical signal; (d) full range EPR spectra with temperature variation.

that reveals the paramagnetic nature of the free radical (Figure 7c and Figure S27a). Along with that, a significant g-shift of the free radical was observed from 100K to 300K. This could be the influence of antiferromagnetic ordering coming from the broad radical signal started appearing from 100K (Figure 7d). The peak-to-peak intensity *vs* temperature plot shows a clear transition of magnetization around 100 to 125 °C, also support the antiferromagnetic exchange from spin-spin interactions of BDPI-units (Figure S27b). Thus, the photomagnetic nature of the photochromic **BDPI-I** is the cumulative effect of paramagnetic and antiferromagnetic species present in the bis(imidazolyl)benzene moiety, that needs further investigation.

Conclusion

A single component and neutral organic molecule was demonstrated to exhibit two very interesting light-induced phenomena such as photochromism and photomagnetism in its pure solid state. Till date, the studies were focused on oxidized form of 1,4-bis(imidazolyl)benzene derivatives for its radical generation and photochromic nature in solution state. For the first time, 1,4-bis(imidazolyl)benzene was shown to exhibit photochromic and photomagnetic behavior in solid-state with the generation of stable π-radicals. Such unprecedented photo-activity in the solid-state was proven by EPR studies which revealed an interesting radical activity in **BDPI**. The solvent molecules, in particular water, found to play a very important role. The hydrogen bonding of water molecules with imidazole N-atoms of BDPI molecules resulted in the strong π-π stacking interactions in **BDPI-I** which in turn promoted the photochromism and radical generation. The relationship between intermolecular interactions and radical generation, followed by photochromism, was clearly established through several chemical modifications of BDPI chromophore and computational analysis. Further, such photoinduced radical activity of **BDPI-I** in the solid state was shown to result in excellent organic photomagnet that exhibits both the paramagnetic and antiferromagnetic features at different temperature. Further studies are under progress in our laboratory to fine tune the 1,4-bis(imidazolyl)benzene chromophore in order to realize their photoinduced paramagnetic and semiconducting properties. This work promises to provide many new insights in the field of stable organic radicals, which are of great utility for the design of optical and sensor devices.

Acknowledgements

We acknowledge the financial support from DST-SERB (CRG/2022/000606), New Delhi, India, and Central Research Facility (CRF) IIT Kharagpur for providing the SCXRD, EPR and SQUID facilities. We acknowledge National Supercomputing Mission (NSM) for providing computing resources of 'PARAM Shakti' at IIT Kharagpur, which is implemented by C-DAC and supported by the Ministry of Electronics and Information Technology (MeitY) and Department of Science and Technology (DST), Government of India. SS thanks CSIR-India for fellowship.

Keywords: Stable Organic Radicals • Photochromism • Photomagnetism • π-stacking • Spin-spin interactions

[1] L. Ji, J. Shi, J. Wei, T. Yu, W. Huang, *Adv. Mater.* **2020**, *32*, 1908015.
[2] Z. X. Chen, Y. Li, F. Huang, *Chem*. **2021**, *7*, 288-332.
[3] B. Tang, J. Zhao, J. Xu, X. Zhang, *Chem. Sci.* **2020**, *11*, 1192-1204.
[4] A. Rajca, *Chem. Rev.* **1994**, *94*, 871-893.
[5] J. P. Peterson, A. Ellern, A. H. Winter, *J. Am. Chem. Soc.* **2020**, *142*, 5304-5313.
[6] S. Kumar, Y. Kumar, S. K. Keshri, P. Mukhopadhyay, *Magnetochemistry*, **2016**, *2*, 42-77.
[7] A. Paul, A. Gupta, S. Konar, *Cryst. Growth Des.* **2021***, 21,* 5473−5489.
[8] X. Hu, H. Chen, L. Zhao, M. Miao, Y. Zheng, *Chem. Mater.* **2019**, *31*, 10256-10262.
[9] M. B. Mills, T. Wohlhauser, B. Stein, W. R. Verduyn, E. Song, P. Dechambenoit, M. Rouzières, R. Clérac, K. E. Preuss, *J. Am. Chem. Soc.* **2018**, *140*, 16904-16908.
[10] Y. Zheng, M.-S. Miao, G. Dantelle, N.D. Eisenmenger, G. Wu, I. Yavuz, M. L. Chabinyc, K. N. Houk, F. Wudl, *Adv. Mater.* **2015**, *27*, 1718-1723.
[11] C. P. Constantinides, E. Carter, D. M. Murphy,; M. Manoli, G. M. Leitus, M. Bendikov, J. M. Rawson, P. A. Koutentis, *Chem. Commun.* **2013**, *49*, 8662-8664.
[12] O. Sato, *Acc. Chem. Res.* **2003**, *36*, 692-700.
[13] O. Sato, J. Tao, Y.-Z. Zhang, *Angew. Chem. Int. Ed*. **2007**, *46*, 2152-2187.
[14] A. Mandal, Y. Li, P. Herson, M. Seuleiman, M.-L. Boillot, E. Riviere, M. Julve, L. Rechignat, A. Bousseksou, R. Lescouezec, *Chem. Commun.* **2012**, *48*, 5653-5655.
[15] J. Glatz, J.-R. Jiménez, L. Godeffroy, H. J. V. Bardeleben, L. Fillaud, E. Maisonhaute, Y. Li, L.-M. Chamoreau, R. Lescouëzec, *J. Am. Chem. Soc.* **2022**, *144*, 10888-10901.
[16] E. Katsnelson, *J. Appl. Phys.* **1991**, *69*, 4556-4558.
[17] V. L. Gurevich, R. Laiho, A. V. Lashkul, *Phys. Rev. Lett.* **2022**, *69*, 180-183.
[18] O. Sato, T. Iyoda, A. Fujishima, K. Hashimoto, *Science* **1996**, 272, 704-705.
[19] L.-Z. Cai, Q.-S. Chen, C.-J. Zhang, P.-X. Li, M.-S. Wang, G.-C. Guo, *J. Am. Chem. Soc.* **2015**, *137*, 10882-10885.
[20] M. Li, M. You, M. Lin, *Dalton Trans.* **2021**, *50*, 4959-4966.
[21] X. Chen, W. Zhao, G. Baryshnikov, *Nat. Commun.* **2020**, *11*, 945-952.
[22] S. Nakatsuji, *Chem. Soc. Rev.* **2004**, *33*, 348-353.
[23] N. Fridman, M. Kaftory, Y. Eichen, S. Speiser, *Journal of Photochemistry and Photobiology A: Chemistry* **2007**, *188*, 25-33.
[24] N. Xie, Y. Chen, *Journal of Photochemistry and Photobiology A: Chemistry* **2007**, *189*, 253-257.
[25] N. Fridman, S. Speiser, M. Kaftory, *Cryst. Growth & Des.* **2006**, *6*, 1653-1662.
[26] S. Roy, S. P. Mondal, S. K. Ray, K. Biradha, *Angew. Chem. Int. Ed.* **2012**, *51,* 12012-12015.
[27] J.-L. Zhao, M.-H. Li, Y.-M. Cheng, X.-W. Zhao, Y. Xu, Z.-Y. Cao, M.-H. You, M.-J. Lin, *Coordination Chemistry Reviews* **2023**, *475,* 214918-214940.
[28] N.-N. Zhang, Y.-F. Han, M.-X. Du, R.-J. Sa, M.-S. Wang, G.-C. Guo *Chem. Eur. J.* **2019**, *25*, 13972–13976**.**
[29] N.-N. Zhang, R.-J. Sa, S.-S. Sun, M.-D. Li, M.-S. Wang, G.-C. Guo, *J. Mater. Chem. C,* **2019**, *7*, 3100-3104.
[30] X.-Q. Yu, M.-S. Wang, G.-C. Guo, *Adv. Funct. Mater.* **2023**, 2212907.
[31] A. Kikuchi, F. Iwahori, J. Abe, *J. Am. Chem. Soc.* **2004**, *126*, 6526-6527.
[32] A. Kikuchi, H. Ito, J. Abe, *J. Phys. Chem. B* **2005**, *109*, 19448-19453.
[33] K. Mutoh, Y. Nakagawa, S. Hatano, Y. Kobayashi, J. Abe, *Phys. Chem. Chem. Phys.* **2015**, *17*, 1151-1155.
[34] D. Davidson, M. Weiss, M. Jelling, *J. Org. Chem.* **1937**, *2*, 319-327.
[35] I. Tiffour, A. Dehbi, A.-H. I. Mourad, A. Belfedal *Materials Chemistry and Physics* **2016**, *178*, 49-56.
[36] J. C.S. Costa, R. J.S. Taveira, C. F.R.A.C. Lima, A. Mendes, L. M.N.B.F. Santos *Optical* Materials **2016**, *58*, 51-60.
[37] Y. Beldjoudi, M. A. Nascimento, Y. J. Cho, H. Yu, H. Aziz, D. Tonouchi, K. Eguchi, M. M. Matsushita, K. Awaga, I. Osorio-Roman, C. P.

Constantinides, J. M. Rawson, *J. Am. Chem. Soc.* **2018**, *140*, 6260-6270.
[38] C. Tansakul, E. Lilie, E. D. Walter, F. Rivera III, A. Wolcott, J. Z. Zhang, G. L. Millhauser, R. Braslau, *J. Phys. Chem. C* **2010,** *114,* 7793–7805.
[39] A. T. John, A. Narayanasamy, K. P. Sudhakaran, M. Hariharan, *Cryst. Growth Des.* **2022**, *22*, 5686−5693.
[40] E. Sebastian, A. M. Philip, A. Benny, M. Hariharan, *Angew. Chem. Int. Ed.* **2018**, *57*, 15696–15701.
[41] Y. X. Zeng, Z. Z. Lai, Y. Han, H. Z. Zhang, S. L. Xie, X. H. Lu, *Adv. Mater.* **2018**, *30*, 1802396.
[42] M. Kalapsazova, S. Ivanova, R. Kukeva, S. Simova, S. Wegner, E. Zhecheva, R. Stoyanova, *Phys. Chem. Chem. Phys.* **2017**, *19*, 27065-27073.
[43] I. Stefaniuk, W. Obermayr, V.D. Popovych, B. Cieniek, I. Rogalska, *Materials* **2021**, *14*, 3449-3460.
[44] Gaussian 09, Revision D.01, M. J. Frisch, G. W. Trucks, H. B. Schlegel, G. E. Scuseria, M. A. Robb, J. R. Cheeseman, G. Scalmani, V. Barone, B. Mennucci, G. A. Petersson, H. Nakatsuji, M. Caricato, X. Li, H. P. Hratchian, A. F. Izmaylov, J. Bloino, G. Zheng, J. L. Sonnenberg, M. Hada, M. Ehara, K. Toyota, R. Fukuda, J. Hasegawa, M. Ishida, T. Nakajima, Y. Honda, O. Kitao, H. Nakai, T. Vreven, J. A. Montgomery, Jr., J. E. Peralta, F. Ogliaro, M. Bearpark, J. J. Heyd, E. Brothers, K. N. Kudin, V. N. Staroverov, T. Keith, R. Kobayashi, J. Normand, K. Raghavachari, A. Rendell, J. C. Burant, S. S. Iyengar, J. Tomasi, M. Cossi, N. Rega, J. M. Millam, M. Klene, J. E. Knox, J. B. Cross, V. Bakken, C. Adamo, J. Jaramillo, R. Gomperts, R. E. Stratmann, O. Yazyev, A. J. Austin, R. Cammi, C. Pomelli, J. W. Ochterski, R. L. Martin, K. Morokuma, V. G. Zakrzewski, G. A. Voth, P. Salvador, J. J. Dannenberg, S. Dapprich, A. D. Daniels, O. Farkas, J. B. Foresman, J. V. Ortiz, J. Cioslowski, D. J. Fox, Gaussian, Inc., Wallingford CT, 2013.
[45] S. Grimme, J. Antony, S. Ehrlich, H. Krieg, *J. Chem. Phys.* **2010**, *132*, 154104-154123.
[46] T. Lu, F. Chen, *J. Comput. Chem.* **2011**, *33*, 580-592.
[47] D. Yuan, W. Liu, X. Zhu, *Chem* **2021**, *7*, 333-357.
[48] Y.-J. Ma, J.-X. Hu, S.-D. Han, J. Pan, J.-H. Li, G.-M. Wang, *Chem. Commun.* **2019**, *55*, 5631-5634.
[49] Deposition numbers 2239861 (for **BDPI-II**) and 2239862 (for **BPI-II**) contain the supplementary crystallographic data for this paper. These data are provided free of charge by the joint Cambridge Crystallographic Data Centre and Fachinformationszentrum Karlsruhe Access Structures service.

Table of Content